Tensor-based Cortical Morphometry via Weighted Spherical Harmonic Representation

Moo K. Chung[1,2], Steve Robbins[4], Kim M. Dalton[2]
Shubing Wang[1], Alan C. Evans[4], Richard J. Davidson[2,3]
[1]Department of Statistics, Biostatistics, and Medical Informatics
[2]Waisman Laboratory for Brain Imaging and Behavior
[3]Department of Psychology and Psychiatry
University of Wisconsin-Madison
[4]Montreal Neurological Institute, McGill University, Canada
mchung@stat.wisc.edu

Abstract

We present a new tensor-based morphometric framework that quantifies cortical shape variations using the local area element. The local area element is obtained from the Riemannian metric tensors, which are, in turn, obtained from the smooth functional parametrization of a triangle mesh. For the smooth parametrization, we have developed a novel weighted spherical harmonic (SPHARM) representation. The weighted-SPHARM differs from the classical SPHARM in a regularizing cost function. The classical SPHARM is a special case of the weighted-SPHARM. Further, for a specific choice of weights, the weighted-SPHARM is shown to be the finite least squares approximation to the solution of an isotropic heat diffusion on a unit sphere. The main aims of this paper are to present a theoretical framework for the weighted-SPHARM, and to show how it can be used in the tensor-based morphometry. As an illustration, the methodology has been applied in the problem of detecting abnormal cortical regions in a clinical population.

1. Introduction

In many previous cortical morphometric studies, cortical thickness have been mainly used to quantify cortical shape variations in a population [11, 13, 14]. The cortical thickness measures the amount of gray matter in the vertical direction on the cortex. We present a new tensor-based morphometry (TBM) that quantifies the amount of gray matter along the tangential direction of the cortex by computing the local area element. The local area element is obtained from the Riemannian metric tensors, which are computed from the smooth functional parametrization of a cortical mesh. For this purpose, we present a novel weighted spherical harmonic (SPHARM) representation that differs from the classical SPHARM [8, 17] in a regularizing cost function. Unlike the classical SPHARM, we weigh measurements in such a way that the closer measurements are weighed more. The weighted-SPHARM is mathematically related to both the classical SPHARM and an isotropic heat diffusion on a unit spher.

Let us overview previous literatures that are related to our study. Gerig et al. (2001) used the mean squared distance (MSD) of SPHARM coefficients in quantifying ventricle surface shape in a twin study [8]. The distance based metrics widely used in deformation-based morphometry do not directly quantify the amount of tissue growth and atrophy [2]. For directly measuring the amount of tissue volume, the Jacobian determinant of the deformation field is a better metric [2]. Our local area element is the differential geometric generalization of the Jacobian determinant. So the area element will be able to quantify the cortical tissue growth/atrophy directly.

Shen et al. (2004) used the principal component analysis technique on the SPHARM coefficients of schizophrenic hippocampal surfaces in reducing the data dimension [17]. Then they classified the hippocampal surfaces using the linear discriminant analysis and a support vector machine. In a related work, Gu et al. (2004) presented the SPHARM representation as a surface compression technique, where the main geometric feasures are encoded in the low degree spherical harmonics, while the noises are in the high degree spherical harmonics [9]. It will be shown that the weighted-SPHARM penalizes high degree spherical harmonics more than the classical SPHARM does.

Bulow (2004) used the spherical harmonics in developing an isotropic heat diffusion via the Fourier transform on a

unit sphere as a form of hierarchical surface representation [1]. We will show that the weighted-SPHARM representation is related to the heat diffusion asymptotically.

Most SPHARM literatures [1, 8, 9, 17] use the both real- and imaginary-valued spherical harmonics. However, the coefficients of imaginary-valued spherical harmonic basis do not serve any purpose in SPHARM representation other than providing mathematical simplicity. In this paper, we will use real-valued spherical harmonics with different normalizing constants than [1, 8, 9, 17].

Once the differentiable parametrization of the cortex is established by the weighted-SPHARM, we can compute the Riemmanian metric tensors and local area element. Many previous differential geometric cortical modeling is based on locally fitting quadratic polynomials [5, 7]. The SPHARM-based global parametrization tend to be computationally expensive compared to the local quadratic polynomial fitting while providing more accuracy and flexibility for hierarchical representation.

2. Preliminary

2.1. Parametrization

Let $\mathcal{M}$ and S^2 be a cortical surface and a unit sphere respectively. $\mathcal{M}$ and S^2 are realized as meshes with more than 80,000 triangle elements [13]. It is natural to assume the cortical surface to be a smooth 2-dimensional Riemannian manifold parameterized by two parameters [6]. This parametrization is constructed in the following way. A point $p = (x, y, z) \in \mathcal{M}$ is mapped onto $u = (u_1, u_2, u_3) \in S^2$ via a deformable surface algorithm that preserves anatomical homology and the topological connectivity of meshes (Figure 1) [13]. Let U be the inverse mapping from S^2 to $\mathcal{M}$. Point $u = (u_1, u_2, u_3) \in S^2$ is parameterized by the spherical coordinates:

$$(u_1, u_2, u_3) = (\sin\theta\cos\varphi, \sin\theta\sin\varphi, \cos\theta)$$

with $(\theta, \varphi) \in \mathcal{N} = [0, \pi] \otimes [0, 2\pi)$. This mapping will be denoted as X, i.e. $X : \mathcal{N} \to S^2$. Then we have composite mapping $Z = U \circ X : \mathcal{N} \to \mathcal{M}$. Z is a 3D vector and it will be stochastically modeled as

$$Z(\theta, \varphi) = \nu(\theta, \varphi) + \epsilon(\theta, \varphi), \tag{1}$$

where ν is unknown true differentiable parametrization and ϵ is a random vector field on S^2. The computation of the Riemannian metric tensors and the local area element require estimating differentiable function ν.

2.2. Spherical harmonic representation

The basis functions on the unit sphere are given as the eigenfunctions satisfying $\Delta f + \lambda f = 0$, where Δ is the spherical Laplacian:

$$\Delta = \frac{1}{\sin\theta}\frac{\partial}{\partial\theta}\Big(\sin\theta\frac{\partial}{\partial\theta}\Big) + \frac{1}{\sin^2\theta}\frac{\partial^2}{\partial^2\varphi}.$$

There are $2l+1$ eigenfunctions, denoted as $Y_{lm}(-l \le m \le l)$, corresponding to the same eigenvalue $\lambda = l(l+1)$. Y_{lm} is called the *spherical harmonic* of degree l and order m [4]. The explicit form of the $2l+1$ spherical harmonics of degree l are given as

$$Y_{lm} = \begin{cases} c_{lm} P_l^{|m|}(\cos\theta)\sin(|m|\varphi), & -l \le m \le -1, \\ \frac{c_{lm}}{\sqrt{2}} P_l^0(\cos\theta), & m = 0, \\ c_{lm} P_l^{|m|}(\cos\theta)\cos(|m|\varphi), & 1 \le m \le l, \end{cases}$$

where $c_{lm} = \sqrt{\frac{2l+1}{2\pi}\frac{(l-|m|)!}{(l+|m|)!}}$ and P_l^m is the associated Legendre polynomials of order m. Unlike many previous SPHARM literatures [1, 8, 9, 17] that used the complex-valued spherical harmonics, we use only real-valued spherical harmonics with different normalizing constants since they are more convenient for a real-valued stochastic model (1).

For $f, h \in L^2(S^2)$, the space of square integrable functions in S^2, the inner product is defined as

$$\langle f, h\rangle = \int_0^{2\pi}\int_0^{\pi} f(\theta,\varphi)h(\theta,\varphi)\, d\mu(\theta,\varphi),$$

where Lebesgue measure $d\mu(\theta,\varphi) = \sin\theta d\theta d\varphi$. With respect to this inner product, the spherical harmonics satisfies the orthonormal condition

$$\int_{S^2} Y_{ij}(p)Y_{lm}(p)\, d\mu(p) = \delta_{il}\delta_{jm},$$

where δ_{il} is the Kroneker's delta.

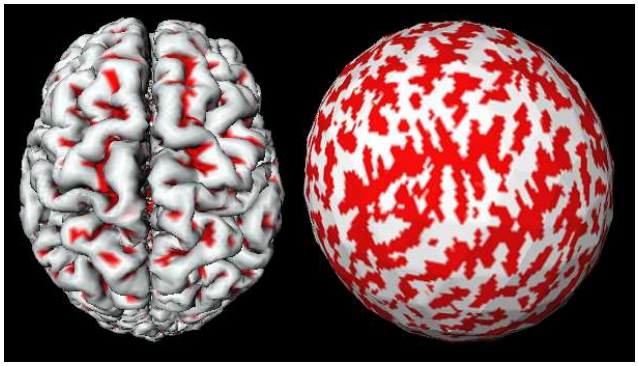

Figure 1. Cortical manifold $\mathcal{M}$ (left) is mapped onto unit sphere S^2 (right) via a deformable surface algorithm that preserves anatomical homology and surface topology [13]. For the visualization purpose, the mean curvature was computed and segmented to better represent sulci and gyri.

Consider subspace

$$\mathcal{H}_k = \{\sum_{l=0}^{k}\sum_{m=-l}^{l} \beta_i Y_{lm} : \beta_i \in \mathbb{R}\} \subset L^2(S^2),$$

which is spanned by up to the k-th degree spherical harmonics. Then the least squares estimation, denoted as $\widehat{f}$, of $f \in L^2(S^2)$ in the subspace $\mathcal{H}_k$ is given by

$$\hat{f}(p) = \sum_{l=0}^{k}\sum_{m=-l}^{l} \langle f, Y_{lm}\rangle Y_{lm}(p).$$

This can be stated as the following theorem.
Theorem 1.

$$\sum_{l=0}^{k}\sum_{m=-l}^{l} \langle f, Y_{lm}\rangle Y_{lm} = \arg\min_{h\in\mathcal{H}_k} \int_{S^2} \big[f(q)-h(q)\big]^2 \, d\mu(q).$$

This theorem is a well known result in Fourier analysis and mainly refered as the genearlized Fourier series expansion. This is the basis of the classical-SPHARM representation for anatomical boundaries [8, 9, 17].

3. Weighted-SPHARM

3.1. Basic theory.

The classical-SPHARM is only one possible representation of functional data measured on the unit sphere. We will present a more general representation technique in the framework of a local kernel regression [10]. We will call this technique as the *weighted-SPHARM* since the coefficients of SPHARM are additionally weighted by the eigenvalues of a kernel. It will be shown that the classical-SPHARM is a special case of the more general weighted-SPHARM representation.

First, we start with the spectral representation of positive definite kernel in S^2. Any positive definite kernel $K(p,q)$ in S^2 can be represented as

$$K(p,q) = \sum_{l=0}^{\infty}\sum_{m=-l}^{l} \lambda_{lm} Y_{lm}(p) Y_{lm}(q), \qquad (2)$$

where eigenvalues $\lambda_{00} \geq \lambda_{1m_1} \geq \lambda_{2m_2} \geq \cdots \geq 0$ satisfy

$$\int_{S^2} K(p,q) Y_{lm}(q) \, d\mu(q) = \lambda_{lm} Y_{lm}(p).$$

This is the special case of the Mercer's theorem [4]. Without loss of generality, we assume the kernel is normalized in such a way that

$$\int_{S^2} K_(p,q) \, d\mu(q) = 1. \qquad (3)$$

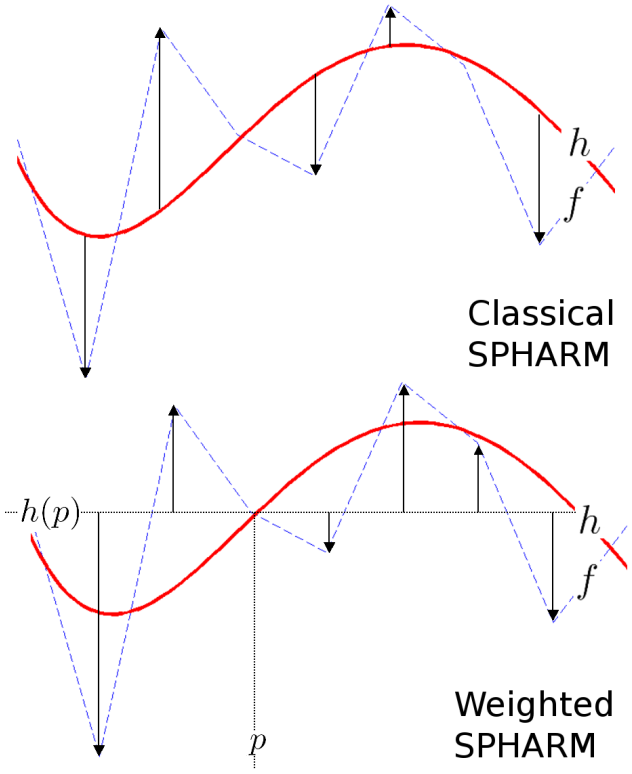

Figure 2. The schematic comparison of the classical-SPHARM and weighted-SPHARM. The classical approach estimates functional data f by minimizing the integrated squared distance between f and smooth function h. This distance is indicated by an arrow. The weighted-SPHARM estimates f locally at each fixed p by minimizing the integrated weighted squared distance between f and $h(p)$. The weighted-SPHARM can be viewed as a local kernel regression [10].

At each fixed point p, smooth representation h of functional data f is searched in the subspace $\mathcal{H}_k$ that minimizes the integral of the weighted squared distance between f and h. This is formulated as the following minimization problem:

$$\min_{h\in\mathcal{H}_k} \int_{S^2} K(p,q)\big[f(q)-h(p)\big]^2 \, d\mu(q). \qquad (4)$$

See Figure 2 for the schematic comparison of the classical SPHARM and the weighed-SPHARM. The minimizer of (4) is given by the following theorem.
Theorem 2.

$$\sum_{l=0}^{k}\sum_{m=-l}^{l} \lambda_{lm}\langle f, Y_{lm}\rangle Y_{lm} = \arg\min_{h\in\mathcal{H}_k} \int_{S^2} K(p,q)\big[f(q)-h(p)\big]^2 \, d\mu(q).$$

Proof. Let

$$h(p) = \sum_{l=0}^{k} \sum_{m=-l}^{l} \beta_{lm} Y_{lm}(p) \in \mathcal{H}_k.$$

The integral can be written as

$$\begin{aligned} & I(\beta_{00}, \beta_{1-1}, \beta_{10}, \beta_{11}, \cdots, \beta_{kk}) \\ = & \int_{S^2} K(p,q) \Big[f(q) - \sum_{l=0}^{k} \sum_{m=-l}^{l} \beta_{lm} Y_{lm}(p) \Big]^2 \, d\mu(q). \end{aligned}$$

Since the functional I is quadratic in coefficients β_{lm}, the minimum exists and it is obtained when

$$\frac{\partial I}{\partial \beta_{l'm'}} = 0 \text{ for all } l' \text{ and } m'. \tag{5}$$

Then solving equation (5) with condition (3), we have

$$\begin{aligned} & Y_{l'm'}(p) \int_{S^2} K(p,q) f(q) \, d\mu(q) & (6) \\ = & \sum_{l=0}^{k} \sum_{m=-l}^{l} \beta_{lm} Y_{lm}(p) Y_{l'm'}(p). & (7) \end{aligned}$$

Integrate the both sides of the equation with respect to measure $\mu(p)$. we obtain

$$\begin{aligned} \beta_{l'm'} &= \int_{S^2} f(q) \, d\mu(q) \int_{S^2} Y_{l'm'}(p) K(p,q) \, d\mu(p) \\ &= \sum_{l=0}^{\infty} \sum_{m=-l}^{l} \lambda_{lm} \int_{S^2} f(q) Y_{lm}(q) \, d\mu(q) \\ &\quad \times \int_{S^2} Y_{lm}(p) Y_{l'm'}(p) \, d\mu(p) \\ &= \lambda_{lm} \int_{S^2} f(q) Y_{l'm'}(q) \, d\mu(q). \end{aligned}$$

This proves the statement.

Now we show what happens as the dimension of $\mathcal{H}_k$ increases. Define kernel smoothing as the integral convolution

$$K * f(p) = \int_{S^2} f(q) K(p,q) \, d\mu(q). \tag{8}$$

Then it can be shown that the weighted-SPHARM converges to kernel smoothing (8) as the dimension of subspace $\mathcal{H}_k$ increases. This can be stated differently as

Theorem 3.

$$K * f(p) = \arg \min_{h \in L^2(S^2)} \int_{S^2} K(p,q) \big[f(q) - h(p) \big]^2 \, d\mu(q).$$

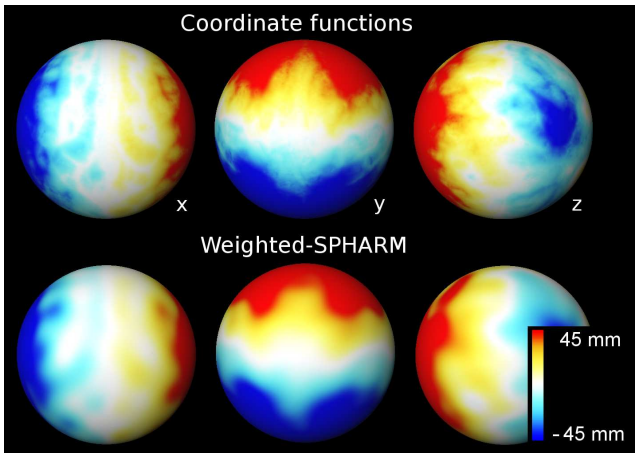

Figure 3. Top: the original inverse mapping U is displayed in S^2. It shows the coordinate functions projected onto S^2. Bottom: the weighed-SPHARM representation of the coordinate functions. The color scale for coordinates is thresholded at ± 45 mm to better show the smoothing pattern of the weighted-SPHARM representation.

Proof. The weighted-SPHARM representation can be rearranged as

$$\begin{aligned} & \sum_{l=0}^{k} \sum_{m=-l}^{l} \lambda_{lm} \langle f, Y_{lm} \rangle Y_{lm}(p) \\ = & \int_{S^2} f(q) \sum_{l=0}^{k} \sum_{m=-l}^{l} \lambda_{lm} Y_{lm}(p) Y_{lm}(q) \, d\mu(q) \\ \to & \int_{S^2} f(q) K(p,q) \, d\mu(q) \quad \text{as } k \to \infty \end{aligned}$$

The last line is from equation (2). On the other hand, from the completeness of Hilbert space $L^2(S^2)$,

$$\begin{aligned} & \lim_{k \to \infty} \arg \min_{h \in \mathcal{H}_k} \int_{S^2} K(p,q) \big[f(q) - h(p) \big]^2 \, d\mu(q) \\ = & \arg \min_{h \in L^2(S^2)} \int_{S^2} K(p,q) \big[f(q) - h(p) \big]^2 \, d\mu(q). \end{aligned}$$

This proves the statement. Theorem 3 connects the weighted-SPHARM to kernel smoothing as the asymptotic limit.

For the choice of eigenvalues $\lambda_{lm} = e^{-l(l+1)\sigma}$, the corresponding kernel is called the *Gauss-Weistrass kernel* and it will be denoted as

$$K_\sigma(p,q) = \sum_{l=0}^{\infty} \sum_{m=-l}^{l} e^{-l(l+1)\sigma} Y_{lm}(p) Y_{lm}(q). \tag{9}$$

The subscript σ is introduced to indicate the dependence of the additional parameter. When $\sigma = 0$, $\lambda_{lm} = 1$ and

the weighted-SPHARM becomes the classical-SPHARM. It is interesting to note that even though the regularizing cost functions are different in Theorem 1 and Theorem 2, they are related. Another interesting property is that $K_\sigma * f$ is the unique solution to the following isotropic diffusion equation

$$\frac{\partial g}{\partial \sigma} = \Delta g, \;\; g(p, \sigma = 0) = f(p) \tag{10}$$

[16]. From this property combined with Theorem 3, we conclude that the weighted-SPHARM is the finite approximation of the isotropic diffusion in S^2.

3.2. Numerical Implementation

We only need to numerically estimate the Fourier coefficients $\langle f, Y_{lm} \rangle$ in the weighted-SPHARM. The eigenvalues λ_{lm} are given analytically from a given kernel. The computation for the Fourier coefficients are based on the direct numerical integration over high resolution triangle meshes with more than 80,000 triangles and the average inter-vertex distance of 0.0189 mm. The accuracy of the weighed-SPAHRM is only restricted to the mesh resolution. Then the Fourier coefficients $\langle f, Y_{lm} \rangle$ is approximated as the Riemann sum over triangle elements. The Riemann sum based approximation should converge to the integral as the mesh resolution increases. The weighted-SPHARM is constructed by iteratively adding each term in Theorem 2.

We have compared the numerical results of the weighted-SPHARM against the analytical solution of (10). Let $f = e^{l'(l'+1)} Y_{l'm'}$ be an analytic test function. Then $K_\sigma * f$ can be written as

$$e^{l'(l'+1)} \sum_{l=0}^{\infty} \sum_{m=-l}^{l} e^{-l(l+1)\sigma} Y_{lm}(p) \int_{S^2} Y_{lm}(q) Y_{l'm'}(q) \; d\mu(q)$$

$$= e^{l'(l'+1)} \sum_{l=0}^{\infty} \sum_{m=-l}^{l} e^{-l(l+1)\sigma} Y_{lm}(p) \delta_{ll'} \delta_{mm'} = Y_{l'm'}(p).$$

The table 1 shows the comparative result for $l' = 20$ and selective m' with $\sigma = 0.01$ and degree $k = 20$. The third column shows the numerical computation of integral

l'	m'	integral	difference
20	4	1.0001	$9.7029 \cdot 10^{-5}$
20	10	0.9999	$1.6212 \cdot 10^{-4}$
20	20	0.9999	$-1.1174 \cdot 10^{-4}$

Table 1. Numerical accuracy of the weighted-SPHARM with $\sigma = 0.01$ for degree 20, and order 4, 10 and 20. The third column checks if $\langle Y_{l'm'}, Y_{l'm'} \rangle = 1$. The last column shows the average difference between the weighted-SPHARM and the expected heat diffusion.

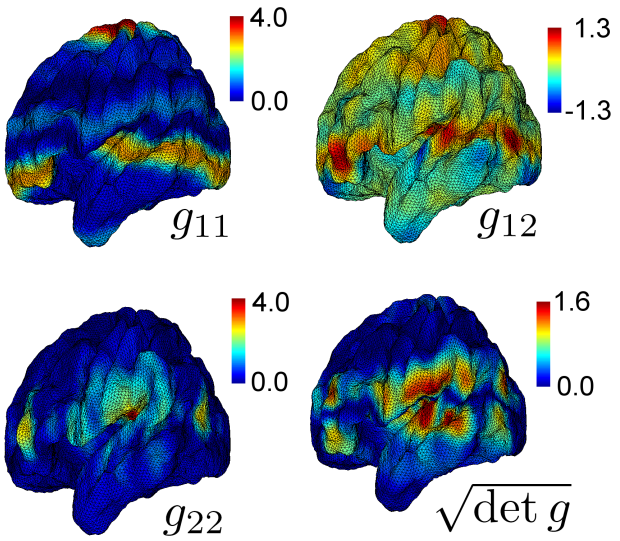

Figure 4. Riemannian metric tensor estimation. The metric tensors g_{ij} are estimated by differentiating the weighted-SPHARM representation. Afterwards the local area element $\sqrt{\det g}$ is computed. The local area element measures the amount of are expansion and shrinking with respect to S^2.

$\int_{S^2} Y^2_{l'm'}(p) \; dp = 1$ showing the accuracy up to 3 decimal places. This shows our Riemann sum approximation provides sufficiently good accuracy, which depends on the mesh resolution. The fourth column shows the average difference between the weighed-SPHARM and the isotropic diffusion.

3.3. Riemannian metric tensor estimation

The weighted-SPHARM estimation $\widehat{\nu}$ of the unknown true parametrization ν in equation (1) is given by

$$\widehat{\nu} = \sum_{l=0}^{k} \sum_{m=-l}^{l} \lambda_{lm} \langle Z, Y_{lm} \rangle Y_{lm}.$$

For this study, we used eigenvalues corresponding to the Gauss-Weistrass kernel. Denoting partial differential operators as $\partial_1 = \partial_\theta$ and $\partial_2 = \partial_\varphi$, we have derivative estimations

$$\partial_i \widehat{\nu} \;\; = \;\; \sum_{l=0}^{k} \sum_{m=-l}^{l} \lambda_{lm} \langle Z, Y_{lm} \rangle \partial_i Y_{lm}(\theta, \varphi).$$

The partial derivatives of spherical harmonics are iteratively computed. The associated Legendre polynomials in the spherical harmonic basis are given by

$$P_l^m(\cos\theta) = \sin^m \theta \frac{d^m}{dx^m} P_l(x) \Big|_{x=\cos\theta},$$

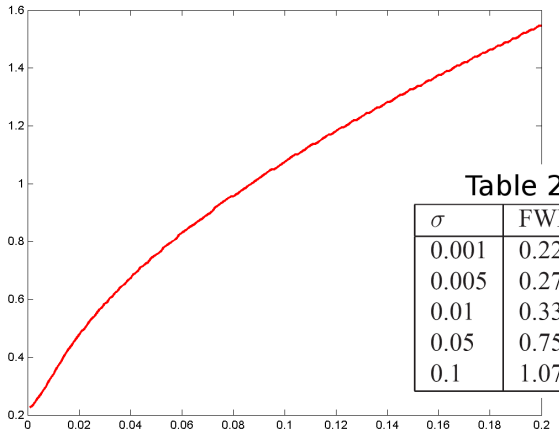

Table 2.

σ	FWHM
0.001	0.2262
0.005	0.2702
0.01	0.3393
0.05	0.7540
0.1	1.0744

Figure 5. Plot of σ (horizontal) vs. FWHM (vertical) showing the nonlinear functional relationship. Table 2. shows FWHM for different σ.

where $P_l(x)$ are the Legendre polynomials defined in $(-1,1)$ with $P_0(x) = 1$ and $P_1(x) = x$. Then for $0 \le m \le l-1$,

$$\begin{aligned}\partial_\theta dP_l^m(\cos\theta) &= m\sin^{m-1}\theta\cos\theta\frac{d^m}{dx^m}P_l(x)\Big|_{x=\cos\theta} \\ &\quad -\sin^{m+1}\theta\frac{d^{m+1}}{dx^{m+1}}P_l(x)\Big|_{x=\cos\theta} \\ &= m\cot\theta P_l^m(\cos\theta) - P_l^{m+1}(\cos\theta).\end{aligned}$$

For $m = l$, since P_l is the l-th order polynomial, the second term vanishes. A similar recursive relationship for an alternate definition for the associated Legendre polynomial is given in [12]. Based on this iterative relation, we can compute the partial derivatives

$$\partial_\theta Y_{lm} = \begin{cases} c_{lm}\partial_\theta P_l^{|m|}(\cos\theta)\cos(|m|\varphi), & -l \le m \le -1, \\ \frac{c_{lm}}{\sqrt{2}}\partial_\theta P_l^0(\cos), & m = 0, \\ c_{lm}\partial_\theta P_l^{|m|}(\cos\theta)\sin(|m|\varphi), & 1 \le m \le l \end{cases}$$

and

$$\partial_\varphi Y_{lm} = \begin{cases} |m|c_{lm}P_l^{|m|}(\cos\theta)\cos(|m|\varphi), & -l \le m \le -1, \\ 0, & m = 0, \\ -|m|c_{lm}P_l^{|m|}(\cos\theta)\sin(|m|\varphi), & 1 \le m \le l. \end{cases}$$

Then the Riemannian metric tensors are estimated as $g = (g_{ij}) = \langle \partial_i\widehat{\nu}, \partial_j\widehat{\nu}\rangle$ and the area element $G(\theta,\varphi) = \sqrt{\det g}$. The area element measures the transformed area in $\mathcal{M}$ of the unit square of the parameterized space $\mathcal{N}$ via mapping ν.

4. Statistical inference in S^2

For the i-th subject ($1 \le i \le m$), we denote the cortical manifold as $\mathcal{M}_i$ and its area element as $G_i(\theta,\varphi)$. The area element is influenced by the global brain size. If we enlarge the cortical coordinates by the factor of r, the area element changes by the factor of r^2. So it is necessary to normalize G_i such that it is invariant under scaling. The affine scale invariant area element is given by

$$\widetilde{G_i}(\theta,\varphi) = \frac{4\pi G(\theta,\varphi)}{\mu(\mathcal{M}_i)},$$

where $\mu(\mathcal{M}_i)$ is the total cortical area. If we enlarge the the cortical coordinates by the factor of r, $\mu(\mathcal{M}_i)$ increases by the factor of r^2 making $\widetilde{G_i}$ invariant under affine scaling. The constant 4π is multiplied so that the normalization is with respect to the total surface area of S^2. Then we have the following general linear model (GLM):

$$\widetilde{G_i}(\theta,\varphi) = \alpha_0 + \alpha_1\cdot \texttt{age}_i + \alpha_2(\theta,\varphi)\cdot \texttt{group}_i + \epsilon(\theta,\varphi),$$

where ϵ is a mean zero Gaussian random field. $\texttt{age}_i$ and $\texttt{group}_i$ are the age and a categorical dummy variable (0 for autism and 1 for control) respectively for subject i. Then we test if there is any group difference in the local area element measure by testing

$$\begin{aligned} & H_0 : \alpha_2(\theta,\varphi) = 0 \text{ for all } \theta \text{ and } \varphi. \\ \text{vs.} \quad & H_1 : \alpha_2(\theta,\varphi) \ne 0 \text{ for some } \theta \text{ and } \varphi. \end{aligned}$$

At each point (θ,φ), a F-statistic with 1 and $n-3$ degrees of freedom, denoted as $F(\theta,\varphi)$ is used as a test statistic. The F-statistic is constructed as a ratio of the residual sum of error of model fit of H_0 and H_1. Since we need to perform the test at every (θ,φ), this becomes a multiple comparison problem. We used the random field theory [18, 19] based thresholding to determine the statistical significance.

The probability of obtaining false positives (α-level) for the one sided alternate hypothesis in given by

$$P(\sup F(\theta,\varphi) \ge F_\alpha) = \sum_{i=0}^{2}\frac{\mathcal{L}_i(S^2)}{\text{FWHM}^i}\rho_i(y),$$

where $\mathcal{L}_i$ is the i-th Lipschitz-Killing curvature or Minkowski functional [18], and ρ_i is the i-dimensional EC-density [19]. FWHM denotes the full width at the half maximum of smoothing kernel K_σ used in the weighted spherical harmonic representation. For the unit sphere, the Lipschitz-Killing curvatures are

$$\mathcal{L}_0(S^2) = 2,\ \mathcal{L}_1(S^2) = 0,\ \text{ and } \mathcal{L}_2(S^2) = 2\pi.$$

The EC-densities are

$$\rho_0(y) = \int_y^\infty \frac{\Gamma(\frac{m}{2})}{((m-1)\pi)^{1/2}\Gamma(\frac{m-1}{2})}\Big(1+\frac{y^2}{m-1}\Big)^{-m/2}\,dy$$

$$\rho_2(y) = \frac{4\ln 2}{(2\pi)^{3/2}}\frac{\Gamma(\frac{m}{2})y\Big(1+\frac{y^2}{m-1}\Big)^{-(m-2)/2}}{(\frac{m-1}{2})^{1/2}\Gamma(\frac{m-1}{2})}.$$

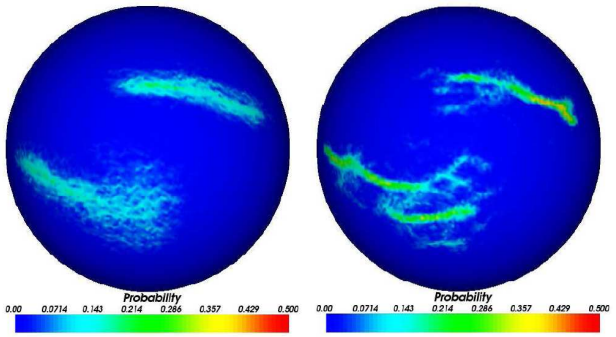

Figure 6. Demonstration of cortical surface normalization in S^2 showing the nonlinear alignment of central and superior temporal sulci for 149 subjects. Left: before normalization. Right: after normalization. The probability of matching increases after normalization.

4.1. Computing FWHM

The computation for the FWHM of the Gauss-Weistrass kernel in S^2 is not trivial due to the fact there is no known close form expression for the FWHM as a function of σ. So the FWHM is computed numerically.

The Gauss-Weistrass kernel can be simplified from equation (9), via the harmonic addition theorem, as

$$K_\sigma(p,q) = \sum_{l=0}^{\infty} \frac{2l+1}{4\pi} e^{-l(l+1)\sigma} P_l^0(\cos\vartheta), \qquad (11)$$

where ϑ is the angle between p and q. Using the vector inner product $\cdot$, the angle can be written as $\cos\vartheta = p \cdot q$. The maximum of the Gauss-Weistrass kernel is obtained when $\vartheta = 0$ and it is given by

$$\sum_{l=0}^{k} \frac{2l+1}{4\pi} e^{-l(l+1)\sigma}.$$

Now we fix $\varphi = 0$ and let p be the north pole, i.e. $p = (0,0,1)$. By varying $q = (\sin\vartheta, 0, \cos\vartheta)$ for $0 \le \vartheta = \cos^{-1}(p \cdot q) \le \pi$, we have $Y_{lm} = 0$ if $m \neq 0$. Note $P_l^0(1) = 1$ for all l. Then we solve numerically for ϑ in

$$\frac{1}{2}\sum_{l=0}^{k} \frac{2l+1}{4\pi} e^{-l(l+1)\sigma} = \sum_{l=0}^{k} \frac{2l+1}{4\pi} e^{-l(l+1)\sigma} P_l^0(\cos\vartheta).$$

The FWHM is then 2ϑ. Table 2 in Figure 5 shows the nonlinear relationship between σ and the corresponding FWHM for $k = 20$.

5. Application to autism study

Three Tesla T_1-weighted MR scans were acquired for 16 autistic and 12 control males. 16 autistic subjects were diagnosed with high functioning autism. The average ages are 17.1 ± 2.8 and 16.1 ± 4.5 for control and autistic groups respectively. Image intensity nonuniformity was corrected using nonparametric nonuniform intensity normalization method and then the image was spatially normalized into the Montreal neurological institute (MNI) stereotaxic space using a global affine transformation. Afterwards, an automatic tissue-segmentation algorithm based on a supervised artificial neural network classifier was used to classify each voxel as cerebrospinal fluid (CSF), gray matter, or white matter. Triangular meshes for outer cortical surfaces were obtained by a deformable surface algorithm [13]. The mesh starts as an ellipsoid located outside the brain and is shrunk to match the cortical boundary. By performing an affine transform on this ellipsoid, we obtain S^2 mesh, which is used in the weighted-SPHARM.

The segmented cortical meshes are normalized via a nonlinear surface-to-surface registration [15]. Cortical curvatures of two surfaces are mapped onto the sphere and they are aligned by solving a regularization problem that tries to minimize the discrepancy between two curvatures while maximizing the smoothness of the alignment in such a way that the pattern of gyral ridges are matched smoothly. This regularization mechanism produces a smooth deformation field, with very little folding. The deformation field is parameterized using a triangulated mesh and the algorithm proceeds in a coarse-to-fine manner, with four levels of mesh resolution. Figure 6 demonstrates the effectiveness of this surface registration algorithm by showing the increased matching probability of superior temporal and central sulci for 149 subjects.

Afterwards, the weighted-SPHARM representation is used as an estimate for differentiable smooth parametrization of the meshes. We used parameters $k = 20$ and $\sigma = 0.001$. The corresponding FWHM is 0.2262 mm. The Riemannian metric tensors and the area element are computed simultaneously. Based on the general linear model framework, the statistical parametric map (F-statistic) is computed and projected on both S^2 and the average cortical surface (Figure 7). The average cortical surface is constructed by averaging the anatomically corresponding vertices in the meshes. It serves as an anatomical landmark for showing where signals are detected. Then we performed the random field theory based multiple comparison correction on the F-statistic at $\alpha = 0.05$ level but we did not detect any statistically significant cortical regions of local area difference although we observed maximum F-value of 9.3 (uncorrected p-value of 0.0054) at the left temporal lobe.

6. Conclusions and discussions

In this paper, we presented a theoretical framework for the weighted-SPHARM and its application in TBM. The weighted-SPHARM is used as a differentiable parametrization of the cortex. This enable us to compute the Rieman-

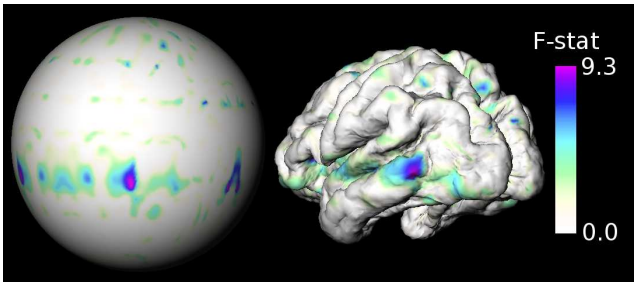

Figure 7. The final statistical analysis result. The F statistic is computed at every vertices of the triangle mesh in S^2 (left) and mapped onto the average cortex (right). The average cortex serves as an anatomical reference. The random field theory based multiple comparison at $\alpha = 0.05$ did not show any significant result although the maximum signal is detected at the left temporal lobe ($\sup F = 9.3$ corresponds to the uncorrected p-value of 0.0054).

nian metric tensors and local area element. The local area element is used in determining the statistical significance of the abnormal cortical tissue expansion/shrinking for a clinical population. Unfortunately, we did not detect any statistically significant signal possibly due to low degree ($k = 20$) used. So it is necessary to increase the computational efficiency using a fast Fourier coefficient estimation technique such as the iterated residual fitting (IRF) [3].

The weighted-SPHARM is a very flexible functional estimation technique for scalar and vector data obtained in S^2. It was shown that the solution to the isotropic heat diffusion in S^2 is the asymptotic limit of the weighted-SPHARM for particular weights. We can extend this argument further. The solution of any linear self-adjoint partial differential equation (PDE) can be expressed as using the weighted-SPAHRM representation so we can avoid using numerical technique such as the finite element method in solving PDEs in S^2. This should serve as a spring board for investigating the wide variety of PDE based data smoothing technique in the kernel regression framework [10].

References

[1] T. Bulow, Spherical diffusion for 3d surface smoothing, *IEEE Transactions on Pattern Analysis and Machine Intelligence*, vol. 26, pp. 1650–1654, 2004. 2

[2] M.K. Chung, K.J. Worsley, T. Paus, C. Cherif, J.N. Giedd, J.L. Rapoport and A.C. Evans. A Unified Statistical Approach to Deformation-Based Morphometry, *NeuroImage* 14:595-606, 2001. 1

[3] M.K. Chung, L. Shen, K.M. Dalton, D.J. Kelley, S.M. Robbins, A.C. Evans, R.J. Davidson, Weighted spherical harmonic representation and its application to cortical analysis. TR 1118. Dept. of Stat., Univ. of Wisconsin-Madison, 2006. 8

[4] R. Courant and D. Hilbert., *Methods of Mathematical Physics, Volume 1.*, Interscience, New York, 1953. 2, 3

[5] A.M. Dale and B. Fischl. Cortical Surface-based Analysis I. Segmentation and Surface Reconstruction. *NeuroImage*, 9:179–194. 1999 2

[6] C. Davatzikos and R.N. Bryan. Using a Deformable Surface Model to Obtain a Shape Representation of the Cortex. In *Proceedings of the IEEE International Conference on Computer Vision*, pages 2122–2127. 1995 2

[7] S. Joshi, U. Grenander, and M.I. Miller, On the geometry and shape of brain sub-manifolds, *International Journal of Pattern Recognition and Artificial Intelligence: Special Issue on Processing of MR Images of the Human*. 11:1317–1343. 1997. 2

[8] G. Gerig, M. Styner, D. Jones, D. Weinberger, J. Lieberman, Shape analysis of brain ventricles using SPHARM. MMBIA 171-178. 2001. 1, 2, 3

[9] X. Gu, Y.L. Wang, T.F. Chan, P.M. Thompson, S.T. Yau. Genus Zero Surface Conformal Mapping and its Application to Brain Surface Mapping, *IEEE Transactions on Medical Imaging*, 23:1–10. 2004 1, 2, 3

[10] J. Fan and I. Gijbels. *Local Polynomial Modelling and Its Applications*. Chapman & Hall/CRC, 1996. 3, 8

[11] B. Fischl, and M.I. Sereno, and R. Tootell, and A.M. Dale, High-resolution intersubject averaging and a coordinate system for the cortical surface *Hum. Brain Mapping*, vol. 8, pp. 272–284, 1999. 1

[12] T. Khan, and A. Thomas. On derivation of the radiative transfer equation and its spherical harmonics approximation for scattering media with spatially varying refractive indices. Technical Report. 2003 6

[13] J.D. MacDonald, N. Kabani, D. Avis and A.C. Evans. Automated 3-D Extraction of Inner and Outer Surfaces of Cerebral Cortex from MRI. *NeuroImage*, 12:340–356, 2000. 1, 2, 7

[14] M.I. Miller, A.B. Massie, J.T. Ratnanather, K.N. Botteron, and J.G. Csernansky. Bayesian construction of geometrically based cortical thickness metrics. *NeuroImage*, 12:676–687, 2000. 1

[15] S.M. Robbins. Anatomical standardization of the human brain in euclidean 3-space and on the cortical 2-manifold. Technical Report PhD thesis, School of Computer Science, McGill University, Montreal, Quebec, Canada, 2003. 7

[16] S. Rosenberg, *The Laplacian on a Riemannian Manifold*, Cambridge University Press, 1997. 5

[17] L. Shen, J. Ford,F. Makedon,A. Saykin, surface-based approach for classification of 3D neuroanatomical structures. *Intelligent Data Analysis*, 8(5). 2004. 1, 2, 3

[18] J. E. Taylor. A Gaussian Kinematic Formula. *Annals of Probability*. 2006. in press. 6

[19] K.J. Worsley, S. Marrett, P. Neelin, A.C. Vandal, K.J. Friston and A.C. Evans. A Unified Statistical Approach for Determining Significant Signals in Images of Cerebral Activation. *Human Brain Mapping*, 4:58–73, 1996. 6